Published in: Journal of Porous Materials (2008), vol.15, iss.4, pp.397-403
Status: Postprint (Author's version)

Characterization of the porous structure of biodegradable scaffolds obtained with supercritical CO_2 as foaming agent

Angélique Léonard[a] • Cedric Calberg[c] • Greet Kerckhofs[d] • Martine Wevers[d] • Robert Jérôme[b] • Jean-Paul Pirard[a] • Albert Germain[c] • Silvia Blacher[a]

[a] *Laboratory of Chemical Engineering, University of Liège, 4000 Liège, Belgium ;* [b] *CERM, University of Liège, 4000 Liège, Belgium ;* [c] *Laboratory of Industrial Chemistry, University of Liège, 4000 Liège, Belgium ;* [d] *Metallurgy and Materials Engineering, Katholieke Universiteit Leuven, 3001 Leuven, Belgium*

Abstract

Poly(ε-caprolactone) foams were prepared, via a batch process, by using supercritical CO_2 as foaming agent. Their porous structure was characterized through mercury porosimetry, helium and mercury pycnometry, scanning electron microscopy (SEM) and X-ray microtomography observations coupled with image analysis. The pore size distributions obtained by these two latter techniques show that the pore structure is more homogeneous when the foaming process is performed under a high CO_2 saturation pressure (higher than 250 bars).

Keywords: Supercritical CO_2 • Foaming agent • Microtomography • Image analysis • 3D images • 3D reconstruction

1. Introduction

Porous polymeric materials are very attractive because they show high flexibility for generating morphologies to meet specific applications. In particular, porous biodegradable polymer matrices are widely used in biomedical applications such as tissue engineering and guided tissue regeneration [1]. These matrices provide a temporary support for cell seeding and growth. They are also used to deliver growth factors to the growing cells. Among biodegradable polymers, poly(*ε*-caprolactone) (PCL) meets all the chemical requirements for tissue engineering [2]. The techniques reported for generating porous PCL foams include freeze-drying and classical foaming processes. However, the main drawback of these techniques is that they respectively require organic solvents and chemical blowing agents during their fabrication processes. Residues of these chemicals left in the polymer after expansion may be harmful to the transplanted cells. Therefore, methods using supercritical CO_2 (sc CO_2) as foaming agent are often preferred, because CO_2 is known as a chemically inert and non-toxic gas [3]. Moreover, as a result of their compressed state, supercritical fluids (SCF) are highly suited to the generation of polymer foams. Solvent free approaches have thus been developed wherein a polymer is saturated with sc CO_2 at high pressure, followed by rapid depressurization at constant temperature. These methods take advantage of the large depression of the glass transition temperature found for many polymers in the presence of sc CO_2, which means that amorphous polymers may be kept in the viscous state at relatively low temperature. In the present work, we explore the preparation and the characterization of neat PCL foams prepared by using sc CO_2 as blowing agent. The same batch process was used in other works allowing the comparison of the results [4, 5, 6]. The obtained foams are made of an isotropic network of pores with a pore size distribution that depends on the experimental variables, such as the pressure and temperature of saturation, the depressurization profile and the composition of the polymer formulation.

The texture characterization of these highly porous materials is a major issue in relation with their potential applications. Mercury porosimetry is traditionally used to characterize this kind of materials. However, it has been shown recently that anisotropic poly(L-lactide-co-*ε*-caprolactone) foams generated by freeze-drying shrink under the high pressure required for Hg intrusion [7, 8]. In this work, the reliability of this technique is discussed when applied to isotropic PCL foams synthesized by expansion of polymer using supercritical CO_2, at various pressures. Additionally, two other complementary and independent characterization techniques were applied: X-ray microtomography and SEM. X-ray microtomography coupled with image analysis was used as a non-destructive alternative method for the 3D characterization of the foams pore texture. Indeed, X-ray microtomography constitutes a promising characterization technique for materials with a high amount of macro- and ultra-macropores, as shown lately for alumina foams [9].

In order to determine the porosity and the pore size distribution of the PCL foams, image analysis was performed on 2D images obtained by scanning electron microscopy (SEM) at high magnification and 3D images obtained by X-ray microtomography at low magnification. It is shown that the pore structure of the studied foams strongly depends on the CO_2 saturation pressure used for the foaming process.

2. Material and methods

PCL used in this study was supplied by SOLVAY (CAPA 650, Mw ~ 50.000). Before foaming, PCL was moulded into sheets of 25 mm diameter and 3 mm thickness at 120°C during 10 min. Basically, foaming was processed in three steps. The samples were first saturated with CO_2 at high pressure and low temperature (40°C) and then kept under these conditions during 2 h. Subsequently, CO_2 was slowly released from the autoclave within 12 min at ambient temperature. The CO_2 pressure of saturation was changed to produce the following four different foams: A1(150 bars), A2 (200 bars), A3 (250 bars) and A4 (300 bars).

The pore size distribution and the total pore volume were determined by mercury porosimetry (Carlo Erba 2000). The Washburn equation [10] was used to calculate the pore diameter, *d*, in relation to the external pressure, P, applied to force mercury, a non-wetting liquid, into the pores. The pore volume was measured in a large pressure range, from ca. 0.15 up to 2000 bars, corresponding to pore diameters ranging from 7.5 nm to 150 µm. The apparent specific volume, V_s, which is the reverse of the bulk density, was measured by mercury pycnometry. After placing a foam sample of weight w_s in a pycnometer, it was completely filled with mercury and weighed (w_{sl}). V_s was calculated according to the expression $V_s = (w_1\text{-}w_{sl} + w_s)/w_s\rho_{Hg})$ where w_1 is the weight of the pycnometer filled with mercury and ρ_{Hg} is the density of mercury (13.5 g cm^{-3}). The specific volume of the solid foam skeleton, V_{sk}, was measured by helium pycnometry (AccuPyc 1330, Micrometrics). The foam porosity was then calculated as $\varepsilon = (V_s\text{-}V_{sk})/V_s$ and the specific pore volume, ρ_p, was obtained from the difference between V_s and V_{sk}. In order to observe their internal pore structure, foams were cut with a razor blade. The sections were mounted on an aluminum stub with a carbon adhesive and then coated with platinum (120 sec, Argon atmosphere). Scanning electron microscopy (SEM) was performed with a Jeol JSM-840A SEM operating at an accelerating voltage of 20kV.

The SEM micrographs were digitized on a matrix of 1024 x 1024 pixels with 256 gray levels. Image analysis was performed using the software 'Aphelion3.6' from Adcis (France). Five images of different areas of the same foam were analyzed.

Microtomography was performed with the Philips HOMX 16 with AEA Tomohawk system. Detailed information about this device can be found in [11]. The X-ray source operated at 72 kV and 0.23 mA. The detector was a 1024 x 1024 10-bit range. The spatial resolution (voxel size) for the different samples was: 0.02 x 0.02 x 0.02 mm for A1, 0.02 x 0.02 x 0.02 mm for A2, 0.013 x 0.013 x 0.013 mm for A3 and 0.015 x 0.015 x 0.015 mm for A4. According to the voxel size, X-ray microtomography allows to quantify the pore texture corresponding to pore diameters from 13 µm up to the sample size. 3D images were obtained by stacking a series of 2D binary cross section images using ANT (Skycan) software.

3. Results

3.1. Mercury porosimetry and pycnometry

Results of mercury porosimetry for the four studied foams are reported in Fig. la and Table 1. A direct comparison of the data collected from mercury pycno-and porosimetry shows that the pore volume (V_{pHg}) measured by mercury porosimetry is systematically smaller than the one measured by pycnometry (see Table 1). This discrepancy led us to investigate the reliability of the mercury porosimetry technique. The underestimation of the pore volume measured by mercury porosimetry may have three origins: (a) the contribution of pores with diameter smaller than 7.5 nm is not taken into account during mercury porosimetry measurements; (b) macropores with diameter smaller than 75 µm shrink under the high pressure required for Hg intrusion into small mesopores and (c) ultramacropores with diameter larger than 75 µm are not evaluated because mercury penetrates before the first measurement is done (i.e. below 0.2 bar).

Published in: Journal of Porous Materials (2008), vol.15, iss.4, pp.397-403
Status: Postprint (Author's version)

Fig 1: *(A) Mercury porosimetry measurements and (B) cumulative pore size distribution for the studied samples*

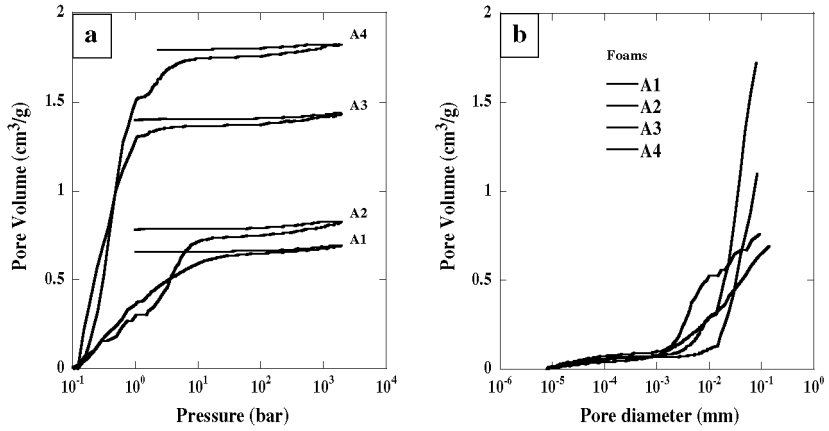

Table 1: *Pycnometry data: Apparent specific volume of the sample (V_s), pore volume (V_p) and foam porosity (ε); Porosimetry data: pore volume (V_{pHg}), volume of mercury (V_{Hg}) and pore volume at 1 bar (V_{res}); Foam porosity determined by X-ray microtomography (δ); Equivalent average pore diameter determined from SEM image analysis (D_{eq})*

Foam	CO_2 pressure (bars)	Pycnometry data (cm^3/g)			Mercury porosimetry data (cm^3/g)			X-ray microtomography data	SEM image analysis data
		^{v}s	^{v}p	ε	^{V}pHg	^{V}Hg	^{V}res	δ	$D\ eq$ (mm)
A1	150	2.47	1.60	0.65	0.69	0.75	0.66	0.62	0.19 ± 0.05
A2	200	2.87	2.00	0.70	0.83	1.16	0.78	0.61	0.23 ± 0.08
A3	250	2.83	1.97	0.70	1.43	1.18	1.40	0.60	0.20 ± 0.06
A4	300	2.96	2.10	0.71	1.82	1.84	1.79	0.60	0.19 ± 0.04

In order to discriminate between these possibilities, the following experiments were carried out, for which the data are reported in Table 1.

1. The pore volume (V_{pHg}) of a foam sample of known weight is measured by mercury porosimetry.

2. The pore volume of the same sample after depressurization at 1 bar (V_{res}) is determined.

3. The sample is weighted after depressurization at 1 bar in order to determine the volume of mercury entrapped (V_{Hg}).

Should the sample collapse when the mercury pressure is raised, V_{Hq} would be much smaller than V_{res}. Since V_{Hq}, V_{res} and V_{pHq} are of the same order of magnitude for the studied samples (see Table 1), we can conclude that the samples were not shrunk but intruded by Hg. Therefore, the contribution to the total pore volume of the pores larger than 75 µm is responsible for the difference between mercury pycno-and porosimetry. It must be noticed that the difference between the pore volume measured by these two methods is maximal for sample A2 and then decreases as the CO_2 foaming pressure increases.

As the accessible pore volume is unchanged during the mercury porosimetry measurement, Washburn equation can be used to calculate the pore size distribution. Figure lb presents the cumulative pore size distribution as measured by mercury porosimetry. For samples Al and A2 pores larger than ca. 1 µm contribute to the pore volume, in particular sample A2 has a larger pore size distribution indicating a less homogeneous structure. For samples A3 and A4, mainly pores larger than ca. 10 µm contribute to the pore volume.

3.2. SEM observations and image analysis

The influence of the CO_2 saturation pressure on the pore structure of PCL foams is shown in Figs. 2a-d. Al foam is composed of two populations of pores: ultramacropores with diameters larger than 1 mm and macropores with

diameters ranging between 50 and 500 µm (Fig. 2a). For the A2 foam, only macropores are present, whose diameters are spread over a larger range (Fig. 2b). Finally, for samples A3 and A4 (Figs. 2c, d), for which the foaming process was performed under the highest CO_2 saturation pressures (250 and 300 bars, respectively) the pore structure is rather homogeneous.

In order to quantify these observations, the pore size distribution was calculated using image analysis techniques. The used image analysis algorithms are described elsewhere [8] and enable the statistical distribution of the equivalent diameter of the pores D_{eq} to be assessed. For the sake of comparison, only macropores smaller than 500 µm were evaluated, *i.e.* ultramacropores observed in the A1 foam were not considered.

For all the samples, a peak is observed in the D_{eq} distribution, which varies from 0.15 to 0.21 mm depending on the CO_2 saturation pressure, but the shape of the distribution is different according to the foaming conditions. The D_{eq} distribution is narrow for foam Al. For foam A2, the distribution spreads towards large values, which could result from a lowering of the size of the ultramacropores observed in Al. Finally, the distribution becomes narrow again for samples A3 and A4 (Fig. 2e). This trend is reflected in the evolution of the mean equivalent diameters and of the standard errors, as presented in Table 1.

3.3. X-ray microtomography and image analysis

According to the results obtained from mercury porosimetry and pycnometry, it appears that pores larger than 75 µm contribute to the total pore volume. As we showed previously [9], X-ray microtomography constitutes a relevant complementary technique to investigate large pore sizes, called 'ultra-macropores'. Typical cross sections of samples Al and A4 are shown in Fig. 3a and b. As the cross-section images present a poor contrast, "tophat" and "bottom-hat" filters [12] were applied together to enhance the contrast. The procedure consisted in adding the original image to the tophat-filtered image, and then subtracting the bottom-hat-filtered image. Then, the resulting image was binarised using Otsu's method [13] (Fig. 3c and d).

With this method, the threshold level is chosen automatically so as to maximize the interclass variance and to minimize the intraclass variance of the thres-holded black (pores) and white (polymer) pixels. Finally, from sets of 100 binary cross sections, 3D binary images of each foam were reconstructed (Fig. 4a, b).

From the 3D processed binary images, the porosity δ, defined as the fraction of voxels of the objects that belong to the pores was measured. It was found that δ was almost constant for all samples (Table 1).

The observation of cross-sections and 3D foams images indicates that the polymer matrix Al (Figs. 3a and 4a) presents a small pores structure, in which a small number of large pores (diameter > 1 mm) are dispersed. For foam A2, the largest pores have disappeared and the pore structure seems denser. Finally, A3 and A4 (Figs. 3b and 4b) present a compact structure.

As the 3D images of foams present a continuous and rather disordered pore structure (Fig. 4) in which it is not possible to assign to each pore a precise geometry, a standard granulometry measurement cannot be applied. Then, to quantify the larger pore sizes, we calculated the opening size distribution [9], which allows assigning a size to both continuous and individual particles. When an opening transformation is performed on a binary image with a structuring element (SE) of size λ, the image is replaced by the envelope of all SEs inscribed in its objects. For the sake of simplicity, spheres of increasing radii λ (approximated by octahedra) were used. When an image is opened by a sphere whose diameter is smaller than the smallest features of its objects, it remains unchanged. As the size of the sphere increased, larger parts of the objects are removed by the opening transformation. Therefore opening can be considered as equivalent to a physical sieving process. This procedure was applied to the reversed 3D images of the foams, i.e. to the 3D images in which pores correspond to white measurable voxels and the matrix to black voxels. Figure 4c shows the volume of the porous network, $G(\lambda)$ normalized by it initial volume, *vs.* the size of the sphere. The comparison of the $G(\lambda)$ distribution for the four foams (Fig. 3c) indicates that the pore size distribution becomes narrower and is also shifted towards smaller sizes when the CO_2 pressure of saturation used in the foaming process increases.

Fig 2: *SEM micrographs for (a) Al, (b) A2, (c) A3 and (d) A4 foams, (e) Pore size distribution obtained by SEM image analysis*

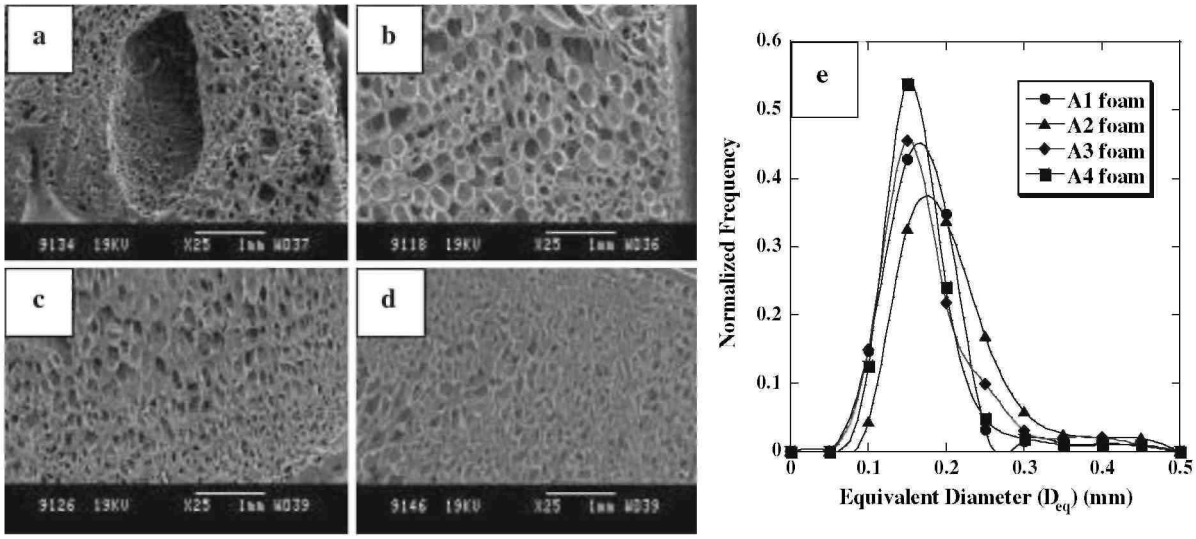

Fig 3: *Tomographic cross section images for (a) A1 and (b) A4 foams and their corresponding binary images (c) and (d)*

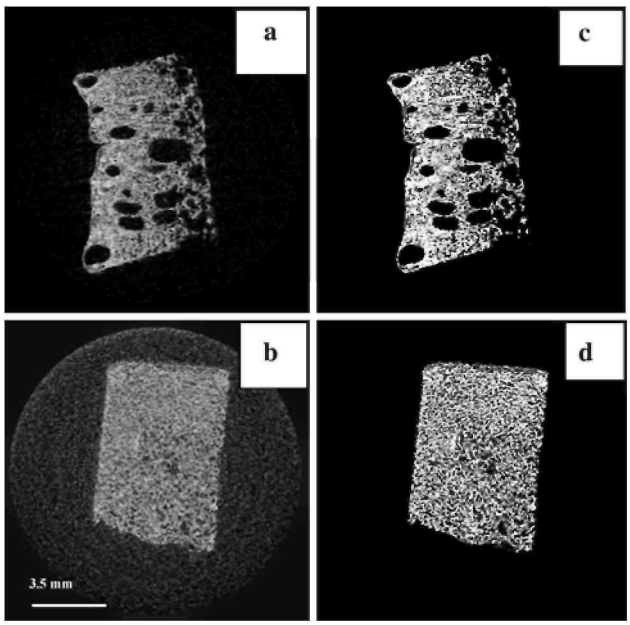

4. Discussion

The pore structure is a key characteristic which must be determined in function of the application. In most cases an homogeneous structure is required. However, in the field of the tissue engineering, foams porosity ideally consists in a bimodal pore distribution in which pores larger than 10 µm are essential for sustaining cell infiltration, whereas pores smaller than 10 µm contribute to cell attachment and create a large surface area for the growth of tissue layer [1, 2,14,15]. In this work, the influence of the sc CO_2 saturation pressure during the foaming process on the pore structure of PCL foams was studied. To achieve this goal, four independent methods were used: mercury porosimetry, helium and mercury pycnometry, SEM, and X-ray microtomography, these two latter techniques being coupled with image analysis. The combination of these techniques allowed extracting information at different scales.

Fig 4: *3D images reconstruction for foams Al (a) and A4 (b). (c) Opening pore size distribution of the studied foams*

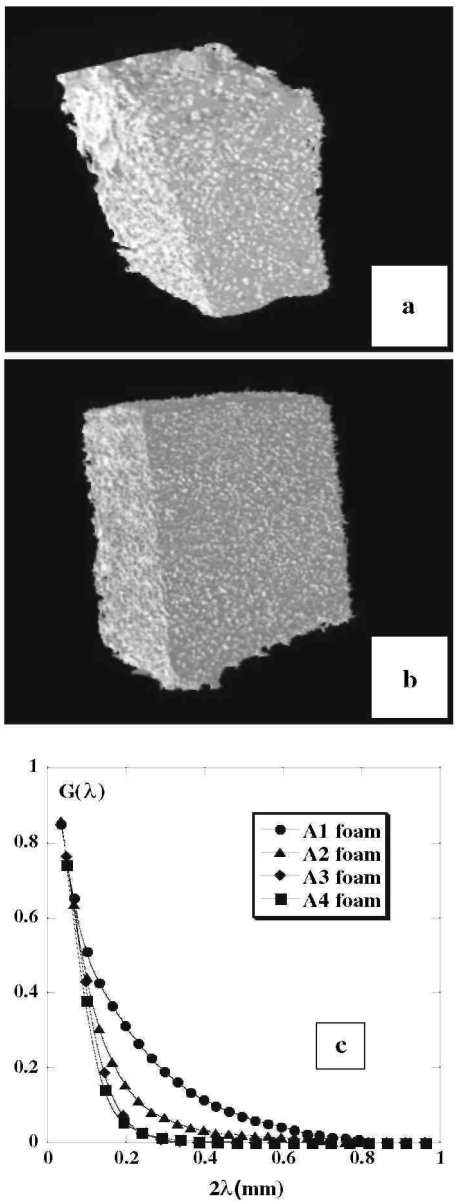

Mercury pycnometry and porosimetry measurements were first performed. As already pointed out [7] possible modifications of the foams pore structure due to the high pressure of mercury could occur. For this reason, a careful analysis of mercury porosimetry data was performed. This analysis shows that the foam density is not modified during the measurement and hence Washburn equation can be applied to determine the pore size distribution. It has been shown that for samples in which the foaming process is performed at the lowest CO_2 saturation pressures (150 bars and 200 bars), the pores larger than 1 µm contribute to the pore volume, whereas for samples prepared at the highest saturation pressures (200 bars and 250 bars) the lower limit of pore size is 10 µm. A comparison between the total pore volume of foams evaluated by mercury pycnometry and porosity measurements indicates the existence of pores larger than 75 µm. The difference between the pore volumes measured by these two techniques is maximal for the sample A2 and then decreases as the CO_2 foaming pressure increases.

To consider the pores beyond the higher limit of mercury porosimetry measurements, SEM and X-ray microtomography observations coupled with image analysis were performed. It is shown that the pore structure becomes more and more homogeneous as foaming CO_2 saturation pressure increases. It is interesting to note that this picture agrees with mercury porosimetry pore distribution for pores smaller than 75 µm. Finally the ultramacropore density of the more open foams (A1 and A2) was determined by X-ray microtomography. The

main advantage of X-ray microtomography lies in its non destructive character, in opposition with SEM that requires the cut of the samples. Moreover, this technique allows to have access to pore sizes higher than 75 µm, the resolution limit of mercury porosimetry. In order to test the ability of microtomography to characterize macro- and ultramacro-porous textures, foaming conditions were selected to obtain pores larger than 10 µm, *i.e.* in the resolution range of the used device.

The porosity of foams evaluated using pycnometry (ε) and X-ray microtomography (δ) agrees well (Table 1). However, the ε values increase with the sc CO_2 saturation pressure between 150 and 200 bar and then level off for higher saturation pressures, whereas the δ values remain almost constant. This difference can be attributed to the combination of those three features: (a) the resolution of the X-ray microtomograph is not sufficient to clearly distinguish the walls from the pores, due the low thickness of the walls and/ or small pore sizes. In this case, it is impossible to discriminate between the gray levels of the those pores and of the polymer matrix which results, at this scale, in a single blurred texture, (b) PCL has a low X-ray attenuation coefficient, which implies to work at relatively low energy level. In our experimental conditions, this leads to a loss of focus stability and to worse detector accuracy, (c) as a result of the poor quality of the images, processing must be performed to enhance the contrast between pores and walls before image binarization. As this processing presents a statistical character, some pixels belonging to pores could be considered as part of the walls and vice-versa, leading to some errors in the quantification of total porosity.

Image analysis of SEM images and of X-ray micro-tomograms shows that the pore size distributions become narrower and is also shifted towards smaller sizes when the foaming CO_2 saturation pressure increases. In particular for sample A1, a continuous distribution in which large pores (~0.8 mm) coexist with small pores (~0.15 mm) is observed.

These results find their origin in the foaming mechanism. The number and size of the formed bubbles is determined by the competition between the rates of bubble nucleation and growth. It is well known from the homogeneous nucleation theory [16] that when the magnitude of the pressure drop induced by the reactor depressurization increases, the energy barrier for nucleation decreases. This leads to an increased nucleation rate, and hence to smaller bubbles. The presence of ultramacropores may be explained by an effect of the temperature. As the temperature drop resulting from the gas expansion is lower for low saturation pressures, the actual temperature following depressurization is higher for Al than for the other samples. In this case, bubbles have much more time to grow. This is prone to favor the coalescence of bubbles.

5. Conclusion

Mercury pycnometry and porosimetry, SEM and x-ray microtomography coupled with image analysis are complementary methods that provide valuable information on the texture of the studied foams. Mercury porosimetry and SEM image analysis show that the pore structure is more homogeneous when the foaming process is performed under a high CO_2 saturation pressure (larger than ~250 bars). X-ray microtomography allows visualizing the structure and measuring the ultramacropore density and size distribution.

Acknowledgements

The authors thank the Ministry of the "Communauté française de Belgique", Belgium (Action de Recherche Concertée 00/05-265) and the Ministry of "Région Wallonne" (DGTRE), Belgium, in the frame of the W.D.U. and WINNOMAT programs for their financial support. A. Léonard is grateful to the FNRS (National Fund for Scientific Research, Belgium) for a Postdoctoral Researcher position.

References

1. D.M. Liu, V. Dixit (eds), Porous materials for tissue engineerig. (Trans Tech Publications Ltd, Uetikon-Zuerich, 1997)

2. V. Maquet, S. Blacher, R. Pirard, J-P. Pirard, R. Jerome, J. Biomed. Mater. Res. Appl Biomater. 43, 291 (1998)

3. A. Cooper, Adv. Mater. 15, 1049 (2003)

4. Qun Xu, X. Ren, Y. Chang, J. Wang, L. Yu, K. Dean, J. Appl. Polym. Sci. 94, 593 (2004)

5. S. Cotugno, E. Di Maio, G. Mensitieri, S. Iannace, G.W. Roberts, R.G. Carbonell, H.B. Hopfenberg, Ind. Eng. Chem. Res. 44, 1795 (2005)

6. F. Stassin, Ph D Thesis, University of Liège, 2005

7. J. Tija, PJ. Moghe, J. Biomed. Mater. Res. Appl. Biomater. 43, 291 (1998)

8. V. Maquet, S. Blacher, R. Pirard, J.-P. Pirard, M.N. Vyakarnam, R. Jérôme, J.B.M.R. Appl Biomater. 66, 199 (2003)

9. S. Blacher, A. Léonard, B. Heinrichs, N. Tcherkassova, F. Ferauche, M. Crine, P. Marchot, E. Loukine, J.P. Pirard, Colloid Surface A. 241, 201 (2004)

10. E.W. Washburn, Phys. Rev. 17, 273 (1921)

11. http://www.mtm.kuleuven.ac.be/Research/Equipment/ Mechanical/MCT.html

12. J. Serra, Image Analysis and Mathematical Morphology. 1 (Academic Press, New York, 1982)

13. N. Otsu, IEEE Trans. Syst. Man Cybern. 9, 62 (1979)

14. J-J. Blaker, JE. Gough, V. Maquet, I. Nothingher, A.R. Boccacini, J. Biomed. Mater. Res. Part A. 67, 1401 (2003)

15. A.R. Boccacini, J.J. Blaker, V. Maquet, R.m. Day, R. Jérôme, Materials Science & Engineering. C25(l), 23 (2005)

16. O.Olabisi, L.M. Robeson, M.T. Shaw, Polymer-Polymer Miscibility. Academic Press, NewYork, (1979)